BBA - Biomembranes 1863 (2021) 183588

Contents lists available at ScienceDirect

BBA - Biomembranes

journal homepage: www.elsevier.com/locate/bbamem

Evaluation of DIBMA nanoparticles of variable size and anionic lipid content as tools for the structural and functional study of membrane proteins

Natalia Voskoboynikova [a], Eleonora Germana Margheritis [b], Felix Kodde [a], Malte Rademacher [a], Maurice Schowe [a], Annette Budke-Gieseking [b], Olympia-Ekaterini Psathaki [b], Heinz-Jürgen Steinhoff [a,*], Katia Cosentino [b,*]

[a] Department of Physics, University of Osnabrück, 49069 Osnabrück, Germany
[b] Department of Biology and Center for Cellular Nanoanalytics (CellNanOs), University of Osnabrück, Germany

ARTICLE INFO

Keywords:
Anionic lipids
Amphiphilic maleic acid-containing polymers
DIBMALPs
Model membranes
Membrane protein complexes

ABSTRACT

Amphiphilic maleic acid-containing polymers allow for the direct extraction of membrane proteins into stable, homogenous, water-soluble copolymer/lipid nanoparticles without the use of detergents. By adjusting the polymer/lipid ratio, the size of the nanoparticles can be tuned at convenience for the incorporation of protein complexes of different size. However, an increase in the size of the lipid nanoparticles may correlate with increased sample heterogeneity, thus hampering their application to spectroscopic and structural techniques where highly homogeneous samples are desirable. In addition, size homogeneity can be affected by low liposome solubilization efficiency by DIBMA, which carries a negative charge, in the presence of high lipid charge density.

In this work, we apply biophysical tools to characterize the size and size heterogeneity of large (above 15 nm) lipid nanoparticles encased by the diisobutylene/maleic acid (DIBMA) copolymer at different DIBMA/lipid ratios and percentages of anionic lipids. Importantly, for nanoparticle preparations in the diameter range of 40 nm or below, the size homogeneity of the DIBMA/lipid nanoparticles (DIBMALPs) remains unchanged. In addition, we show that anionic lipids do not affect the production, size and size homogeneity of DIBMALPs. Furthermore, they do not affect the overall lipid dynamics in the membrane, and preserve the functionality of an enclosed membrane protein.

This work strengthens the suitability of DIBMALPs as universal, native-like lipid environments for functional studies of membrane proteins and provide useful insight on the suitability of these systems for those structural techniques requiring highly homogeneous sample preparations.

1. Introduction

Membrane proteins are central to the cellular functions, including the activation of signaling cascades, the selective in and out passage of ions and nutrients, and for cell-to-cell communication [1]. However, their structural characterization lags behind that of soluble proteins due to the challenge of extracting and handling them when isolated from the membrane environment.

Lipid/polymer nanoparticles stabilized by amphiphilic maleic acid (MA)-containing copolymers, such as styrene/maleic acid (SMA) or the SMA-related diisobutylene/maleic acid (DIBMA) copolymers, represent the latest methodological advance in the model membrane field for their ability to directly extract membrane proteins from artificial or natural membranes [2–4]. These copolymers self-insert into the lipid bilayer and, at suitable concentrations, extract proteins, together with their lipid surrounding, into disc-shaped MA/lipid particles (SMALPs or DIBMALPs), without the need for detergents [5]. This represents a clear advantage over conventional approaches (including classical nanodiscs obtained by membrane scaffold proteins, MSP) as it preserves the native membrane environment [3,6]. Besides, they are particularly suitable for the extraction of membrane proteins and protein complexes whose macromolecular architecture could be destroyed during detergent removal or addition [7,8].

Depending on the polymer used and the protocol, this technology

* Corresponding authors.
E-mail addresses: hsteinho@uni-osnabrueck.de (H.-J. Steinhoff), katia.cosentino@uni-osnabrueck.de (K. Cosentino).

https://doi.org/10.1016/j.bbamem.2021.183588
Received 6 December 2020; Received in revised form 15 February 2021; Accepted 17 February 2021
Available online 1 March 2021

allows for the extraction of homogenous lipid particles that can be tuned in size [9] [10]. Control over particle size allows for the incorporation of a defined number of protein units and lipids. This approach turns particularly advantageous for the study of membrane proteins in their native membrane environment by all spectroscopic and structural techniques that require water-soluble, homogeneous lipid nanoparticles of uniform composition, such as cryo-electron microscopy [5] [11,12].

SMALPs are typically characterized by a narrow size distribution centered around a diameter range of 10–12 nm [13–15]. DIBMA has the advantage over SMA to enable a milder fragmentation of membranes resulting in larger lipid particles, whose size range from 10 up to 50 nm depending on the lipid/polymer ratio [16]. Unlike SMALPs, this striking characteristic of DIBMALPs should allow for i) a higher degree of freedom for protein conformational changes to occur and ii) the accommodation of big proteins or even protein complexes, thus offering great opportunities for their structural characterization in a native membrane environment [14,17]. However, so far, not much information is available on the size homogeneity and lipid dynamics in DIBMALPs, likely due to the increase in size heterogeneity correlating with the production of larger nanoparticles.

In addition, it has been shown that the size of DIBMALPs is strongly affected by both the length and the degree of unsaturation of the lipid chains [9]. However, it is not clear how DIBMA, which carries a negative charge, behaves in the presence of an increasing amount of anionic lipids, which are present at different amounts in plasma and intracellular membranes and are thought to be important contributors in protein binding, insertion and assembly in the membrane bilayer [18–20] [21].

Here, we investigate the size, size homogeneity and lipid dynamics of DIBMALPs of large size (above 15 nm) obtained by different polymer/lipid ratio and lipid composition (Fig. 1).

By using dynamic light scattering (DLS), transmission electron microscopy (TEM) and atomic force microscopy (AFM), we found that up to 20% of dimyristoyl phosphatidylserine (DMPS) lipids do not affect the size and size homogeneity of DIBMALPs of variable size compared to pure dimyristoyl phosphatidylcholine (DMPC) lipid systems. Besides, we observed that the homogeneity of DIBMALPs is affected only by DIBMA/lipid ratios producing particles above 40 nm in diameter, while below this value (corresponding to DIBMA/lipid mass ratios of 1 or higher), nanoparticle preparations presented comparable size heterogeneity. Under these conditions, for all analyzed DMPS concentrations, DIBMALPs had a size variability of ±7–9 nm, which is relevant information when designing experimental approaches that require homogeneous samples for structural studies.

By using spin-labeled lipid electron paramagnetic resonance (EPR) spectroscopy, we investigated the dynamics of lipids in 20% DMPS DIBMALPs prepared using different DIBMA/lipid ratios. EPR data showed that the mobility of spin labeled lipids in the membrane bilayer of DIBMALPs is unaffected neither by the presence of anionic lipids nor by the size of the nanoparticles. Furthermore, we took the light-sensitive membrane protein sensory rhodopsin II (*Np*SRII) as a case study to investigate functional aspects of membrane proteins enclosed in DIBMALPs with anionic lipids. We found that the photochemical reactions of *Np*SRII reconstituted in DIBMALPs are very similar to those found in nanodiscs [22]; thus, *Np*SRII retains its functionality in DIBMA-stabilized anionic-lipid nanoparticles.

2. Materials and methods

2.1. Chemicals

1,2-Dimyristoyl-*sn*-glycero-3-phosphocholine (DMPC) was a kind gift from Lipoid (Ludwigshafen, Germany). 1,2-Dimyristoyl-*sn*-glycero-3-phospho-L-serine (DMPS), 1-palmitoyl-2-stearoyl-(5-doxyl)-*sn*-glycero-3-phosphocholine (16:0–5 doxyl PC), 1-palmitoyl-2-stearoyl-(12-doxyl)-*sn*-glycero-3-phosphocholine (16:0–12 doxyl PC) and 1-palmitoyl-2-stearoyl-(16-doxyl)-*sn*-glycero-3-phosphocholine (16:0–16 doxyl PC) were purchased from Sigma-Aldrich (St. Louis, MO, US). DIBMA copolymer, commercially available under the trade name as PureCube DIBMA 10 in TRIS (lyophilized in Tris-buffer, pH 7.5), was bought from Cube Biotech, Germany. All other reagents were of analytical grade.

2.2. Protein purification

For purification purposes, *Np*SRII has a C-terminal 6xHis-tag. *Np*SRII-His was expressed in *E. coli* BL21 (DE3) cells and purified according to [23–25] with minor modifications. Briefly, transformed cells were grown in Luria-Bertani (LB) medium containing 50 mg/ml kanamycin at 37 °C to an optical density OD_{580} of 1.0. The overexpression of the protein was induced by addition of IPTG to a final concentration of 0.5 mM. 10 μM all-trans retinal (Sigma) was also added. After an induction period of 3 h at 37 °C, cells were harvested (4200 g; 15 min; 4 °C), washed and resuspended (1/100 culture volume) in 150 mM NaCl, 25 mM NaPi (pH 8.0), 2 mM EDTA buffer containing a protease inhibitor mix. Cells were disrupted by sonication (Branson Sonifier II W-250, Heinemann, Germany). Membranes were isolated by centrifugation (50,000g; 1 h; 4°C), and solubilized in buffer A (300 mM NaCl, 50 mM NaPi (pH 8.0), 2% (w/v) DDM) overnight at 4 °C. Solubilized membrane proteins were isolated by centrifugation (50,000g; 1 h; 4°C) followed by chromatography using Ni-NTA superflow material which was pre-equilibrated with buffer B (300 mM NaCl, 50 mM NaPi (Na_2HPO_4/NaH_2PO_4) pH 8.0, 0.05% (w/v) DDM). Non-specifically bound proteins were removed by washing extensively with buffer B containing 30 mM imidazole. His-tagged protein was eluted with buffer B containing 200 mM imidazole. Fractions containing the desired protein were pooled and dialyzed against buffer C (500 mM NaCl, 10 mM Tris (pH 8.0), 0.05% (w/v) DDM)) to remove imidazole. If not used directly for reconstitution, protein samples were flash frozen and stored at −80 °C. Protein concentrations were determined using an UV-VIS spectrophotometer

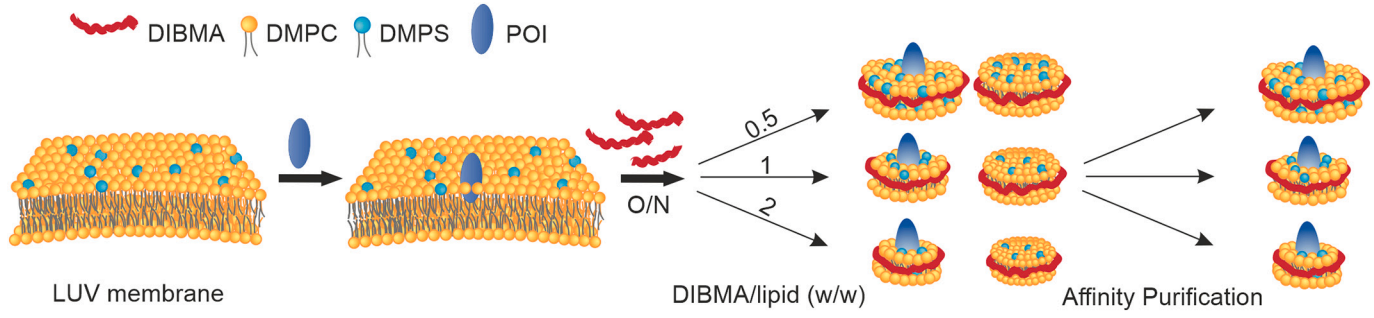

Fig. 1. Scheme of preparation of DIBMALPs with and without incorporated proteins. Large unilamellar vesicles (LUVs, 100 nm) at defined lipid composition of DMPC/DMPS (mol%) were incubated overnight (O/N) with DIBMA copolymer resulting in the assembly of DIBMALPs. When specified, nanoparticles containing a protein of interest (POI) were produced by incorporating the POI in the LUVs before DIBMA addition. Nanoparticles containing the POIs were purified to isolate them from the empty ones.

(UV-2450, Shimadzu Corporation, Kyoto, Japan). The concentration of *Np*SRII was determined by using the known extinction coefficient of 50,000 M^{-1} cm^{-1} at $\lambda = 280$ nm.

2.3. Vesicle preparation

Large unilamellar vesicles (LUVs) composed of either DMPC or DMPC and DMPS at defined DMPC/DMPS ratio (mol%) were prepared by suspending dry lipid powders in chloroform to a final lipid concentration of 7.37 mM and, if necessary, mixing with 1 mol% of lipid spin labels (5-, 12- or 16- doxyl PC). Chloroform was evaporated under a stream of nitrogen gas. The resulting lipid film was dried under vacuum for at least 2 h. The dried lipids were suspended in 50 mM Tris (pH 7.5), 200 mM NaCl buffer (Buffer D) and vortexed. Subsequently, the multilamellar liposome suspension underwent five freeze–thaw cycles (N_2/water bath at 37 °C), and, if not used directly, was stored in aliquots at −80 °C. Before reconstitution, the suspension of liposomes was extruded 31 x through polycarbonate membranes (Whatman) of 100 nm pore size using a Mini-Extruder Set (Avanti Polar Lipids, Alabaster, AL, USA) to get unilamellar vesicles.

2.4. Proteoliposome preparation

Proteoliposomes were prepared as published before [22] with minor modifications. Briefly, preformed 100 nm liposomes were equilibrated by stirring for 3 h with n-dodecyl-β-D-maltopyranoside (DDM) at room temperature with a lipid to detergent mixing ratio of 1: 1 (mol/mol). Before adding the protein solution, the lipid-detergent mixture was placed in an ultrasonic bath at room temperature for 10 min. Then *Np*SRII was mixed with the equilibrated DDM-lipid mixture at a molar protein to lipid ratio of 1:172 (equivalent to 5:1 (w/w)) and incubated for 30 min with gentle shaking. To remove the detergent, the reconstitution of the *Np*SRII into liposomes was carried out using hydrophobic polystyrene beads SM-2 Bio-Beads (Bio-Rad Laboratories; Munich; Germany). These hydrophobic polystyrene beads were washed thoroughly beforehand with methanol and water followed by buffer D. The Bio-Beads were added to the protein-lipid detergent solution at a ratio of 10: 1 (w/w) of the wet Bio-Beads to detergent. The samples were incubated for 1 h at room temperature. A new portion of Bio-Beads was then added, and the samples were incubated at 4 °C overnight with gentle shaking. After removing Bio-Beads, the proteoliposomes were collected by centrifugation (126,000*g*; 30 min; 4 °C). Finally, they were resuspended in buffer D to a final lipid concentration of 7.37 mM.

2.5. Preparation of DIBMALPs

Preparation of DIBMALPs was performed as published before [15]. Briefly, to form DIBMA/lipid particles, a 4% (w/v) aqueous solution of DIBMA copolymer was added dropwise to the liposome suspension to get a required final lipid-to-copolymer mass ratio of 2:1, 1:1 and 1:2 at a defined lipid composition of DMPC/DMPS. The assembly mixture was allowed to equilibrate for 1 h at room temperature and then for 16 h at 4 °C. The resulting samples were centrifuged (15,800*g*; 30 min; 4 °C) to remove insoluble aggregates. If necessary, the samples were concentrated using 3 kDa MWCO Vivaspin 500 ultrafiltration devices (Sartorius, UK).

2.6. Thin-layer chromatography (TLC)

In order to verify the composition of lipids in the DIBMALPs, lipids were extracted after nanoparticle formation. Briefly, 200 µl chloroform and 100 µl methanol were added to 100 µl of each DIBMALP preparation and mixed extensively. The samples were then centrifuged (20,000*g*; 10 min; 4 °C) to achieve phase separation. After water phase removal, 8 µl of the chloroform/methanol phase were added to a TLC silica gel plate. DMPS and DMPC were separated upon migration in the mobile phase chloroform: methanol: ammonium hydroxide (65:25:4 v:v:v) by capillary forces in a developing glass jar. The separations were visualized after iodine staining. The separated spots were compared to reference DMPS and DMPC spots. Relative migration Rf values for DMPC and DMPS were then determined.

2.7. Preparation of DIBMALPs containing NpSRII

To form DIBMALPs containing *Np*SRII (in the following abbreviated as *Np*SRII-DIBMALPs), a 4% (w/v) aqueous solution of the DIBMA copolymer was added dropwise to the suspension of proteoliposomes in order to obtain a final copolymer/lipid mass ratio of 1. The mixture was then equilibrated for 1 h at room temperature and then at 4 °C for 16 h. The samples were centrifuged (15,800*g*; 30 min; 4 °C) to remove insoluble aggregates. The resulting samples were then incubated for 1 h at room temperature with gentle agitation with Ni^{2+}-NTA agarose (Qiagen), which had previously been equilibrated with buffer E (300 mM NaCl, 50 mM NaPi (Na_2HPO_4/NaH_2PO_4), pH 8.0). Atypically bound material was removed by washing with 40 mM imidazole in buffer E. DIBMALPs containing His-tagged *Np*SRII were eluted with 200 mM imidazole in buffer E and if necessary dialyzed against buffer D.

2.8. Dynamic light scattering

Dynamic light scattering (DLS) measurements were performed on a Zetasizer Nano ZS (Malvern Instruments, Worcestershire, UK) at 550 nm and 25 °C. Data represent the average of three sets of 14 runs of 10 s each. The particle size distribution was obtained by using the ZETASIZER software package Ver. 7.02. under the assumption that lipid nanoparticles were spherically shaped.

2.9. Transmission electron microscopy

DIBMALPs (2 mg lipid/ml) was diluted 1:100 in buffer D and 4 µl were applied onto negatively glow- discharged carbon-coated 400 mesh copper grids for 1 min. Excess liquid was removed by blotting with filter paper. The grid was washed twice shortly with buffer and stained 4 min with 2% uranyl acetate and blotted. Digital micrographs were collected using a JEM2100Plus Transmission Electron Microscope (JEOL, Japan) operated at 200 kV equipped with a XAROSA CMOS 20 Megapixel Camera (EMSIS GmbH, Germany). The size of DIBMALPs was estimated using the Fiji software [26]. The size corresponds to the diameter of particles, and in case of elliptical shape, to the major axis.

2.10. Atomic force microscopy

For AFM imaging, 250 µl of a solution of DIBMALPs was put in contact with freshly cleaved mica, previously glued to a coverslip, and diluted with additional 250 µl of buffer D. The DIBMALP sample was incubated for 10 min, then mica was washed 3 times with 500 µl of the buffer and then allowed to equilibrate at room temperature before analysis.

DIBMALPs were imaged using a JPK NanoWizard II system (JPK Instruments, Berlin, Germany) mounted on an Olympus IX71 Inverted Microscope (Olympus). Intermittent contact (IC or tapping) mode images were taken using an SNL-10 V-shaped silicon nitride cantilevers (Bruker) with a typical spring constant of 0.06 N/m. The cantilever oscillation was tuned to a frequency between 3 and 10 kHz, and the amplitude was set between 0.3 and 0.7 V. The amplitude was varied during the experiment to minimize the force of the tip on the particles. The scan rate was set to 0.3–0.7 Hz. Images were processed by the JPK processing software, applying a smoothing function. Lipid nanoparticles thickness was measured based on the height profiles from the mica (taken as 0 nm). The size of DIBMALPs was estimated by the JPK processing software. The size corresponds to the diameter of particles, and in case of elliptical shape, to the major axis.

2.11. Statistics

Statistical significance for experiments in Figs. 3 and 4 was obtained with unpaired *t*-test. *P* values ($P < 0.001$) were calculated with Prism 5.0 from GraphPad. Data were obtained from at least two independent measurements.

2.12. Electron paramagnetic resonance spectroscopy

Electron paramagnetic resonance (EPR) measurements were performed as described previously [27]. Briefly, room temperature continuous wave (cw) EPR spectra were recorded on a home-built EPR spectrometer equipped with a dielectric resonator (Bruker Biospin, Germany). Glass capillaries of 0.9 mm inner diameter were filled with sample volumes of ~20 μl. The measurements were recorded at 9.686 ± 0.005 GHz in a B-field range from 3400 G to 3520 G using a B-field modulation amplitude of 0.2 mT. The temperature during the measurements was 295 K.

2.13. Transient optical absorption spectroscopy

Transient optical absorption experiments were carried out as described previously [28]. A 50 W halogen lamp with an infrared cutoff filter (KG-2) and either 400 nm, 500 or 550 nm interference filters illuminated the sample-filled quartz cuvette inside a sample holder, which was temperature-controlled to 298 K. The transmitted light was passed through an interference filter and detected using a photodiode, while a flashlight with a flash duration of 80 μs equipped with a 475 nm edge filter provided excitation perpendicular to the transmission beam. The amplified signal was recorded with an analog-to-digital converter connected to a standard PC. For the transitions between the late photocycle intermediates ($\tau > 2$ ms) studied here, the kinetics determined by flashlight excitation were indistinguishable from those determined by pulsed laser excitation [27]. The transient absorption changes were recorded on samples buffered in 50 mM Tris, pH 7.50, 200 mM NaCl at concentrations of approximately 5 μM.

3. Results

3.1. Increasing concentrations of anionic lipids do not disturb DIBMALPs production

Due to electrostatic repulsion, high lipid charge density might lead to low liposome solubilization efficiency by DIBMA. To test whether the increasing amount of anionic lipids affects DIBMALPs production, size and size homogeneity, we prepared large unilamellar vesicles (LUVs) with increasing concentrations of the negatively-charged lipid DMPS, in the physiological range of 0–20% (mol%), and solubilized them with DIBMA copolymers at different DIBMA/lipid ratios (Fig. 1). The different ratios produced lipid nanoparticles of different size, as measured by dynamic light scattering (Fig. 2A), in agreement with previous findings [16]. At the selected DIBMA/lipid ratios, we obtained lipid nanoparticles from 20 up to 60 nm in diameter, confirming the ability of DIBMA to produce bigger lipid nanoparticles than SMA, which can be instrumental for the accommodation of big molecules and protein complexes in their native environment.

For all lipid compositions tested, we could successfully produce DIBMALPs, although in some samples we noticed the presence of big lipid nanoparticles aggregates (see also TEM and AFM results below). Also, for all lipid compositions, the size of the lipid nanoparticles decreased with increasing the amount of DIBMA (Fig. 2A and C), indicating that, even when electrostatic repulsion in our setting was maximized (highest DIBMA and DMPS concentrations), DIBMA was still able to solubilize the LUVs. Therefore, we concluded that the DIBMA copolymer is suitable for the production of lipid nanoparticles containing variable anionic lipid concentrations mimicking the physiological negative charge density of biological membranes.

3.2. The homogeneity of DIBMALP preparations is not affected by increasing concentrations of anionic lipids and DIBMA/lipid ratios

Using the DLS data alone, we could not observe any difference in the size and size heterogeneity (provided by the polydispersity index, PDI) of DIBMALPs with increasing DMPS concentrations (Fig. 2A and B). Of note, we observed that solubilized DIBMALP samples presented 3- to 4-fold higher polydispersity index (PDI) compared to the narrow size distribution observed for the LUV samples from which they were generated (Fig. 2B and C). This increase was particularly enhanced for the samples at 0.5 DIBMA/lipid ratio, while the 1 and 2 DIBMA/lipid ratio samples presented comparable PDI (Fig. 2B). This indicates that, below a size threshold of 40 nm, nanoparticle preparations have comparable size homogeneity despite their different sizes. Size homogeneity of lipid nanoparticles is a highly relevant parameter for the successful investigation of samples by several spectroscopic and structural techniques. To further investigate the extent of this heterogeneity, the shape of the DIBMALPs and the presence of aggregates, we employed TEM on the DIBMALP samples which showed lower PDI in the DLS measurements, namely at 1 and 2 DIBMA/lipid ratio (Fig. 3A). TEM images of negatively stained DIBMALP samples showed isolated and, to a lesser extent, aggregated disc-shaped lipid nanoparticles, with no significant difference in shape amongst the analyzed lipid compositions (Fig. 3A). In agreement with the DLS data, increasing concentrations of DMPS had

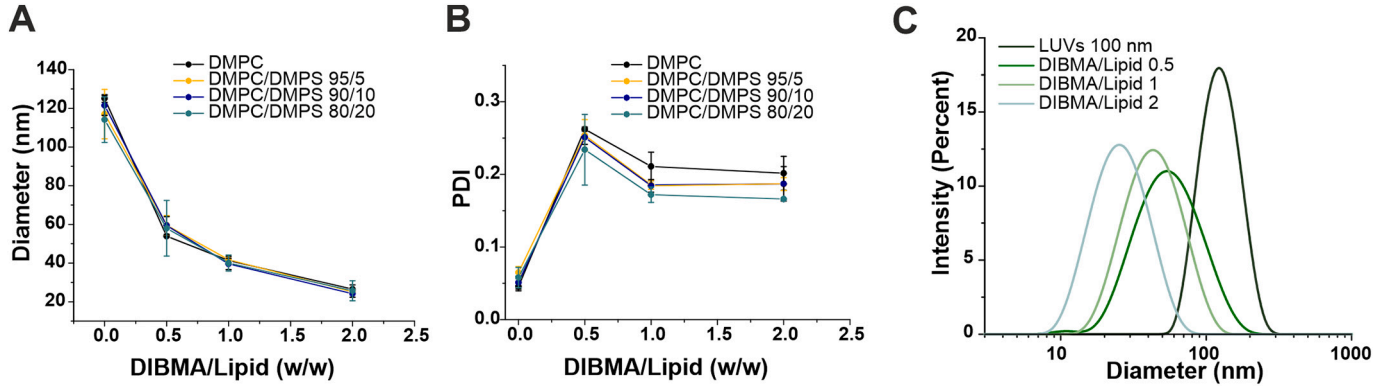

Fig. 2. Lipid negative charge does not alter size and size homogeneity of DIBMALPs as revealed by DLS measurements. A–B) *Z*-average hydrodynamic diameter (A) and polydispersity index (PDI) (B) obtained from DLS measurements of 7.37 mM lipids with the indicated composition (see legend in the graph) titrated with DIBMA (w/w). Error bars are the SD from at least 3 independent preparations. C) Representative DLS intensity-weighted distributions of the hydrodynamic nanoparticle diameter before and after addition of DIBMA to DMPC/DMPS (80:20 mol%) LUVs as reported in A and B.

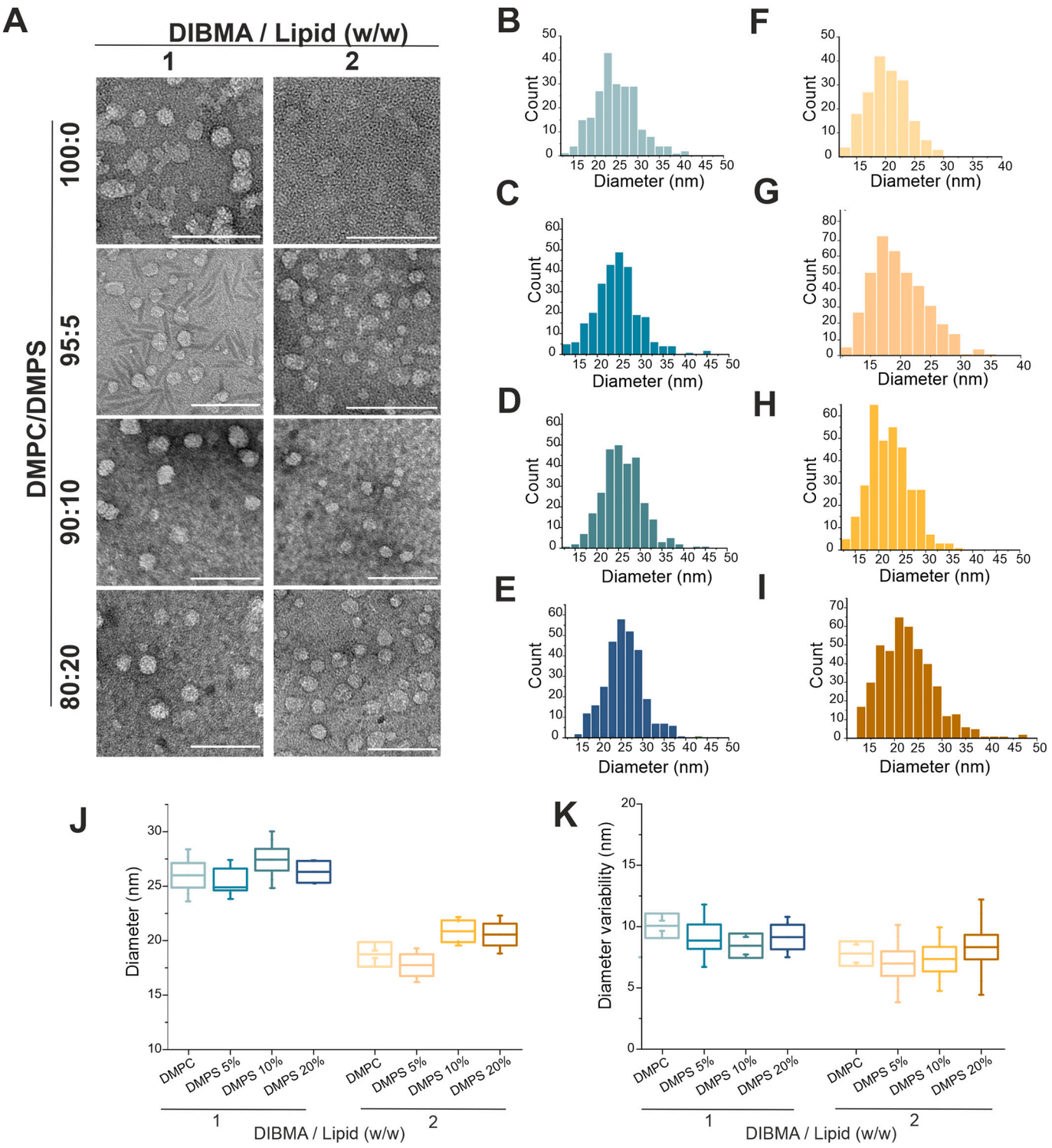

Fig. 3. Structural analysis of DIBMALPs with increasing concentrations of negatively charged lipids. A) Gallery of representative TEM images of DIBMALPs at indicated DIBMA/Lipid (w/w) and DMPC/DMPS (mol%) ratios. Scale bar 100 nm. B–I) Representative size distribution (diameter) of DIBMA/Lipid nanoparticles with DIBMA/Lipid (w/w) = 1 (B-E) or DIBMA/Lipid (w/w) = 2 (F–I) at DMPC/DMPS (mol %) 100:0 (B,F), 95:5 (C,G), 90:10 (D,H), 80:20 (E,I) based on TEM data. J–K) Average diameter (J) and diameter variability (K) of DIBMALPs from size distributions like in B–I. Horizontal lines in the box plot are the average from at least two independent experiments. Images and size distributions are representative of at least two independent experiments.

no effect on the size and size homogeneity of DIBMALPS (Fig. 3B–I). At all analyzed DMPS concentrations, DIBMALPs had an average diameter of 25–27 nm and 17–21 nm for 1 and 2 DIBMA/lipid ratio, respectively (Fig. 3J). Although TEM data provided smaller diameter values than DLS, they are consistent with the DLS data in that the size heterogeneity did not significantly increase for the larger DIBMALPs, varying ±7–9 nm in diameter for both analyzed DIBMA/lipid ratios (Fig. 3K). These findings are in agreement with other studies describing the size heterogeneity of DIBMALPs and seems to be independent of the lipid composition [15,29].

To further characterize the lipid nanoparticles of bigger dimensions, we employed atomic force microscopy (AFM) for DIBMALPs with a

DIBMA/lipid ratio of 1 and compared DMPC with DMPC/DMPS (80:20 mol%), presenting the highest tested percentage of DMPS (Fig. 4). Similar to the TEM micrographs, AFM images in solution showed individual and aggregated disc-shaped lipid nanoparticles. Aggregates, similar to disc piles, occurred more repeatedly in the DMPC samples, while the DMPC/DMPS (80:20 mol%) nanoparticles looked more homogeneously distributed on the glass support, likely due to charge repulsion between interacting bilayers (Fig. 4A and C). For both lipid compositions, the height of DIBMALPs ranged between 3 and 4 nm above the glass support (Fig. 4B and D), demonstrating that, at the tested lipid nanoparticle size, the DIBMA belt does not alter, but retains, the typical lipid-bilayer thickness (~4 nm). Average DIBMALPs diameters were 28.63 ± 11.74 nm and 27.28 ± 15.60 nm for DMPC and DMPC: DMPS (80:20 mol%) lipid composition, respectively (Fig. 4E–G). This data are consistent with the TEM results of a DIBMALPs size distribution varying in a range of ±10 nm and confirm that the lipid charge does not affect the size of DIBMA/lipid nanoparticles.

3.3. The dynamics of spin-labeled lipids in DIBMALPs is hardly affected by the presence of negatively charged lipids

Using EPR spectroscopy we determined the mobility of spin labeled lipids for DIBMALPs with DMPC/DMPS (80:20 mol%), prepared from different DIBMA/lipid ratios, and compared the results with those obtained using nanoparticles without charged lipids [15]. The EPR line shape directly reflects the mobility of the nitroxide bound either to the 5th, 12th or 16th carbon atoms of the host phosphatidylcholine chain, 5-, 12-, and 16-doxyl PC (in the following abbreviated 5-doxyl PC, 12-doxyl PC and 16-doxyl PC) (Fig. 5A). Reorientational correlation times in the ps regime typical for unrestricted reorientational motion of a nitroxide in low viscous media result in three equally spaced sharp lines of similar amplitude. Reorientational correlation times in the ns time scale or spatial restriction of the nitroxide reorientational motion reveal spectra with increased linewidth and apparent hyperfine splitting. For both DMPC and DMPC/DMPS (80:20 mol%) lipid nanoparticles, the EPR spectra showed a gradual decrease of the line broadening and hyperfine splitting when comparing 5-, 12-, and 16-doxyl PC (Fig. 5B).

The apparent hyperfine splitting and, thus, motional restriction is

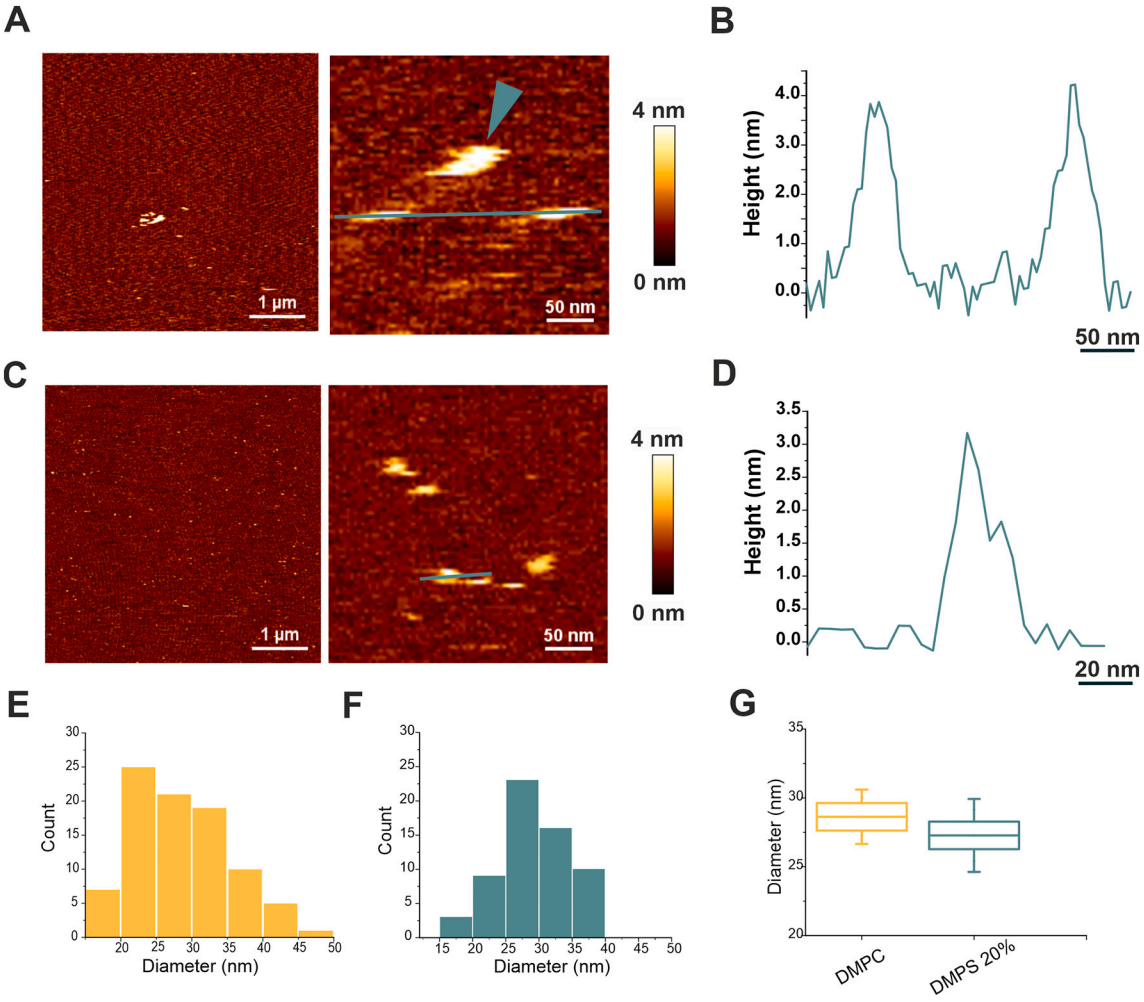

Fig. 4. AFM structural analysis of DIBMALPs with negatively charged lipids. A) Representative AFM images, at different magnification, of DMPC lipid nanoparticles at 1:1 DIBMA/Lipid (w/w) ratio. Scale bar 1 µm (left) and 50 nm (right). The green arrowhead indicates the presence of lipid nanoparticle stacks. B) Height profile corresponding to the green line in the 2D image in A) crossing individual lipid nanoparticles. The height of the nanoparticles (with respect to the mica support) corresponds to the thickness of a typical lipid bilayer (4 nm). C) Representative AFM images, at different magnification, of DMPC/DMPS 80:20 (mol %) lipid nanoparticles at 1:1 DIBMA/Lipid (w/w) ratio. Scale bar 1 µm (left) and 50 nm (right). D) Height profile corresponding to the green line in the 2D image in A) crossing an individual lipid nanoparticle. E–F) Representative size distribution (diameter) of DIBMALPs (DIBMA/Lipid (w/w) = 1) for DMPC (E) and DMPC/DMPS 80:20 (mol %) (F) based on AFM data. G) Average diameter of DIBMALPs from size distributions like in E-F. Horizontal lines in the box plot are the average from at least two independent experiments (dots). Images and size distributions are representative of at least two independent experiments. (For interpretation of the references to color in this figure legend, the reader is referred to the web version of this article.)

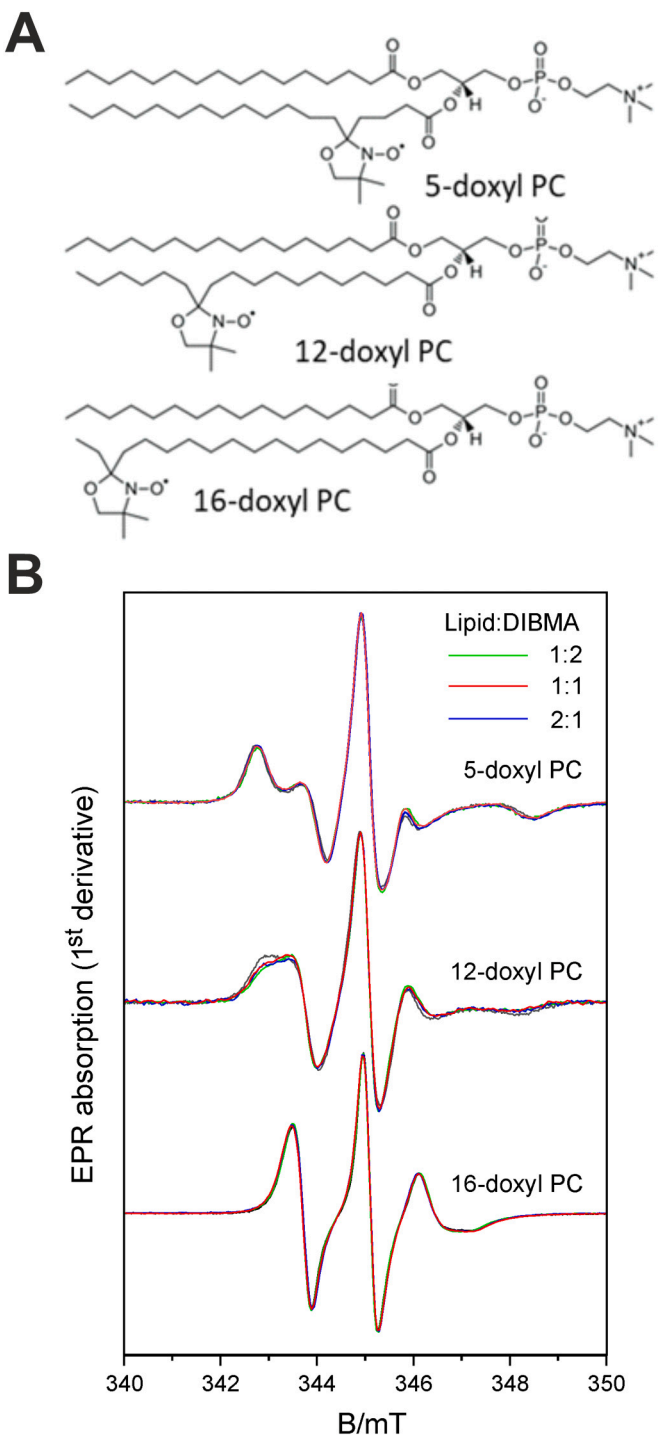

Fig. 5. Dynamics of lipids in DIBMALPs of different composition and size. A) The structures of the spin labeled lipids 5-doxyl PC, 12-doxyl PC and 16-doxyl PC display the positions of the bound nitroxides. B) The corresponding EPR spectra measured in DIBMALPs prepared with different lipid:DIBMA ratios (colored) reveals that, in the given range, lipid dynamics is not influenced by nanoparticle size. The comparison with the spectra recorded from DMPC only DIBMALPs (black) shows that only 12-doxyl PC reports a very slight impact of the charge on the dynamics.

largest for 5-doxyl PC with the nitroxides located close to the lipid head groups and smallest for 16-doxyl PC with the nitroxide located close to the center of the bilayer. The superimposed spectra are nearly indistinguishable revealing that the dynamics at both sites is not significantly influenced by the presence of charged lipids. The spectra of 12-doxyl PC with the nitroxide located close to the center of the lipid monolayer reports slightly increased lipid dynamics in the presence of DMPS. A similar result was reported for 12-doxyl PC in POPC DIBMALPs [15], however, the influence of DMPS is much less pronounced. Therefore, we conclude that for the analyzed lipid nanoparticle sizes, the presence of negatively charged lipids does not have any significant impact on the dynamics of lipids in the membrane bilayer.

3.4. The photocycle of NpSRII reveals its function in DIBMALPs with charged lipids

The light-induced reaction cycle, the so-called photocycle of *Np*SRII, triggers signal transduction in the photoreceptor/transducer complex, *Np*SRII/*Np*HtrII, of *Natronomonas pharaonis* [30] (Fig. 6A). The photocycle kinetics is susceptible to changes of environmental conditions like lipid composition, temperature and pH [7,30,31] and is therefore a sensitive tool for probing protein function. Here, we performed flash-photolysis to study the influence of the DIBMA-lipid (1:1 ratio) environment on the receptor. The light-induced transient absorption changes with the corresponding global multi-exponential fits are shown for three characteristic wavelengths (400, 500 and 550 nm, Fig. 6B). The decay of intermediate M is monitored at 400 nm, the formation and decay of the O-state are followed at 550 nm, and the transients monitored at 500 nm represent the recovery of the *Np*SRII initial state. The time constants from the multi-exponential fits are given in Table 1 in comparison to the corresponding values found for *Np*SRII in nanolipoprotein particles (NLPs) made of *E.coli* lipid extract using MSP1E3D1 as a scaffold protein [22]. Considering error margins, the corresponding values are very similar for these samples, as is already obvious from the comparison of the optical density traces compared in Fig. 6B.

It has been shown that the decay of intermediate M for *Np*SRII in NLPs made of *E.coli* lipid extract is governed by time constants τ_7 and τ_8, also the decay of intermediate O and the recovery of the initial state are determined by these two-time constants [22]. In comparison with the data of NLPs, the decay of intermediate M is slightly accelerated for *Np*SRII in DIBMALPs with 20% DMPS (cf. Fig. 6B), reflected also in a smaller value of τ_7, which is shifted into the direction of the behavior of *Np*SRII in purple membrane lipids (cf. [22]). The present data show that the photocycle kinetics of *Np*SRII, reconstituted in DIBMALPs in the presence of 20% DMPS, is very similar to that found in NLPs, and thus *Np*SRII retains its functionality in DIBMA stabilized lipid nanoparticles.

4. Discussion

Here, we combine several biophysical approaches to compare the size, particle homogeneity and lipid dynamics of DIBMA lipid nanoparticles of tuned size containing negatively charged lipids to evaluate their suitability as a platform for the structural studies of membrane proteins. Previously, nanodiscs of controlled size, in the 6–8 nm diameter range, were obtained by truncated versions of membrane scaffold proteins and characterized for the study of membrane proteins by NMR [33]. The DIBMALPs investigated here present two striking characteristics that make them appealing as a universal platform for membrane protein structural studies: i) a bigger size compared to widely employed nanodiscs and SMALPs, which allows for the integration of big proteins and protein complexes, and ii) the presence of anionic lipids, which is often a requirement for the membrane binding of positively charged proteins through electrostatic attraction. We used different percentages of the anionic lipid DMPS in a range of 0–20% (mol%) to mimic the composition of the plasma membrane and intracellular membrane of different mammalian cells [20] [21].

Previous studies showed the ability of DIBMA copolymers to extract natural membranes [4,16,34] [35], however, they were pointing to enrichment in neutral lipids [35], suggesting that DIBMA may be selective for specific lipids. Although we have no direct evidence that DMPS molecules are evenly distributed in the DIBMALPs, we obtained

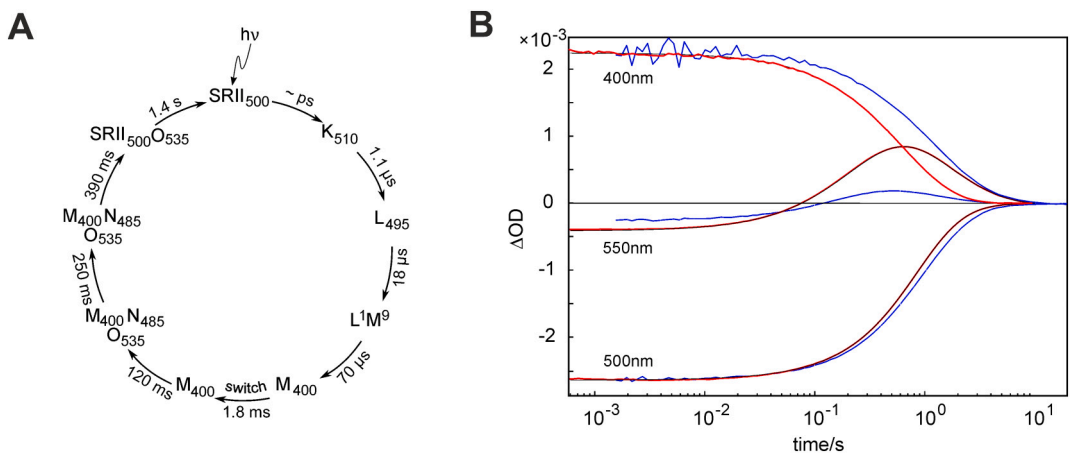

Fig. 6. *Np*SRII receptor retains its functionality in DIBMALPs with negatively charged lipids. A) *Np*SRII photocycle characterized by transient changes in the optical absorption spectrum of the retinal chromophore. Subscripts indicate the wavelength of maximum absorption of the intermediates in nm (adapted from [30]). Time constants for the transitions between these intermediates are given according to the values for *Np*SRII reconstituted in purple membrane lipids [32]. B) The transient optical absorption changes of *Np*SRII in DIBMALPs (DIBMA/lipid ratio 1:1) containing 20% DMPS (red) were recorded at 400 nm (M-intermediate), 500 nm (initial state) and 550 nm (O-state). The three-exponential fits are depicted in solid black. For comparison the corresponding traces of *Np*SRII in NLPs made of *E.coli* lipid extract (data taken from [22]) are given (blue). (For interpretation of the references to color in this figure legend, the reader is referred to the web version of this article.)

Table 1
Photocycle time constants[a] of *Np*SRII reconstituted in different nanoparticles.

*Np*SRII reconstituted in	τ_6/ms	τ_7/s	τ_8/s
DIBMALPs (80% DMPC: 20% DMPS) *Np*SRII:DIBMA:lipid = 1:5:5	270 ± 7	0.69 ± 0.04	2.00 ± 0.16
NLPs (*E.coli* lipid extract) [22]	172 ± 7	0.83 ± 0.07	2.87 ± 0.14

[a] Time constants were averages determined from three preparations of DIBMALPs which contained in addition 1 mol% of either 5-, 12-, or 16-doxyl PC.

high solubilization of the liposomes by DIBMA at all tested lipid compositions, as stated by DLS measurements, where no or little residual peaks corresponding to non-solubilized liposomes were observed for the DIBMA/Lipid (w/w) ratios of 1 and 2 (Fig. 2C). In addition, thin-layer chromatography (TLC) analysis confirmed the presence of DMPS in the DIBMALPs (Supplementary Fig. 1). This suggests that DIBMA does not select zwitterionic over anionic lipids, at least for the investigated percentages of anionic lipids. Rather, the presence of anionic lipids in DIBMALPs supposedly reduces particle aggregation compared to DMPC samples, as verified by both TEM and AFM measurements (Figs. 3 and 4). Our DLS, TEM and AFM analysis indicate that the presence of negatively charged phospholipid headgroups leaves the size and size homogeneity of DIBMALPs unaffected compared to DMPC-only samples. This information adds on to previous findings comparing DMPC and POPC DIBMALP samples [15], highlighting that the acyl chain unsaturation, rather than the lipid charge, affects DIBMALP size. It would be interesting to test the effect of lipid geometry, such as conical phosphatidylethanolamine (PE) or the anionic cardiolipin (CL) on DIBMALP size.

Taking advantage of the ability of DIBMA over SMA copolymers to allow for milder fragmentation, we tested how increasing the size of DIBMALPs affects the heterogeneity of particles of large dimensions (above 15 nm in diameter). We observed that for particle preparations below 40 nm in size, the size homogeneity of DIBMALPs as measured by DLS and TEM, was comparable at all tested conditions (Figs. 2b and 3K). At the light of previous studies showing similar polydispersity for DMPC-only DIBMALPs of smaller size (14 nm in diameter) [15], we conclude that the size of DIBMALPs has a minor or no effect on the size heterogeneity of particles.

Our EPR experiments provided relevant insights into the dynamics of lipids in large DIBMALPs in the presence of anionic lipids. Compared to liposomes, doxyl PCs in polymer-stabilized lipid nanoparticles of small dimensions (below 15 nm) reveal slightly increased motional restrictions [15]. Especially nitroxide positions close to the center of the lipid monolayer report higher-ordered nitroxides as monitored by 10-doxyl PC [36], 11-doxyl PC [37] and 12-doxyl PC [15,38]. This effect is more pronounced in SMALPs than in DIBMALPs. Molecular dynamics simulations provided evidence that spin-labeled lipids tend to relocate to the polymer belt and that the nitroxide moieties of 12-doxyl PC intercalate between the aromatic rings of SMA [15]. Generally, experimental order parameter and reorientational correlation time values of doxyl-PCs in DIBMALPs closely resemble those of doxyl PCs in liposomes more than SMALPs [15]. The presence of charged lipids (Fig. 5) in DIBMALPs does not show any significant influence on the lipid dynamics for the headgroup region or the center of the bilayer. A slight increase of nitroxide dynamics is obvious only for lipid chain position 12 indicating a decreased strength of interaction of this site with the polymer belt.

Finally, the presence of anionic lipids in DIBMALPs does not influence the functionality of the membrane protein *Np*SRII. Recently, it has been shown an additional role of negatively charged lipid DIBMALPS in stabilizing the structure of α-synuclein protein [29]. Overall, these data highlight the very relevant aspect of large DIBMALPs to allow complete protein conformational freedom and lipid dynamics. Of course, this implies tuning the DIBMALPs size based on the size of the target protein or protein complex. From our analysis, DIBMALPs between 20 and 40 nm size can be controllably obtained while keeping a size heterogeneity in the range of 7–9 nm in diameter. In comparison to the narrow size distributions for SMALPs or MSP nanodiscs reported in the literature (with a size variability of around 2–3 nm) [15,39], DIBMALPs result quite heterogeneous in particle size. Whether this size variability can be considered negligible for structural studies of membrane protein complexes where highly homogeneous samples are required, is largely dependent on the specific investigative method as well as on the characteristics of the target protein or protein complex. Considering that a single transmembrane helix has a surface area of about 80 Å^2 [33], a size variability of about 10 nm in the DIBMALPs diameter would result in a variable number of accommodated proteins in the order of several tens of protein units, significantly contributing to sample heterogeneity. However, a fine adjustment of the nanoparticle/membrane protein ratio may allow to gain control over the average number of inserted (non-oligomeric) membrane proteins per nanoparticle thus helping reducing sample heterogeneity, as recently highlighted in a study on MSP

nanodiscs [42]. Furthermore, for large protein complexes, this size variability might be not sufficient for the accommodation of an additional complex. For example, in the case of pore-forming protein complexes, the overall size of the protein pore structure might reach several tens of nanometers [40].

In case of very large protein complexes, tuning the lipid nanoparticle size can additionally turn useful to limit the accommodation of complex units, thus helping to dissect the structural and functional characteristics of individual components [41].

Overall, our study provides relevant insight into the physical properties of DIBMALPs containing negatively charged lipids and on the fluidity of its belt-delimited lipid bilayer. This work reinforces the suitability of DIBMALPs for manifold applications in functional studies of membrane proteins, including single units up to bigger complexes, and provide useful insight on the adaptability of these systems for structural techniques, like cryo-EM, which require highly homogeneous samples.

Supplementary data to this article can be found online at https://doi.org/10.1016/j.bbamem.2021.183588.

Author contribution

K.C., H.-J.S., and N.V. designed the study. N.V. performed protein expression, purification and reconstitution, prepared samples of DIBMALPs and characterized them by DLS with the help of E.G.M. E. G. M. performed the TLC experiments. E.G.M., A.B.G. and O.E.P. performed the TEM experiments. K.C. performed the AFM experiments. F.K. and M. R. performed the EPR experiments and fitted the EPR spectra. M.S. performed the transient optical absorption experiments. K.C. analyzed the DLS, TEM and AFM data. H.-J.S. analyzed the EPR data and interpreted the EPR results. K.C., H.-J.S., and N.V. wrote the draft version of the manuscript. K.C., H.-J.S. completed the final version of the manuscript. All authors read, edited, and approved the final version of the manuscript.

Declaration of competing interest

The authors of the manuscript declare that they have no known competing financial interests or personal relationships that could have appeared to influence the work reported in this paper.

Acknowledgements

The authors thank John Danial for carefully reading the manuscript. This work was supported by German Research Foundation (DFG, STE640/15) to H.J.S, (DFG, SFB 944/3 – 2020, P 26) to K.C. and (DFG, SFB 944 *Z*-Project) to O.E.P. The TEM and AFM imaging was performed in the electron microscopy and optical imaging unit of Integrated Bioimaging Facility (iBiOs) at the Center of Cellular Nanoanalytics (CellNanOs), University of Osnabrück.

References

[1] G. Von Heijne, The membrane protein universe: what's out there and why bother? J. Intern. Med. 261 (6) (2007) 543–557.
[2] S.C. Lee, S. Khalid, N.L. Pollock, T.J. Knowles, K. Edler, A.J. Rothnie, O. R.T. Thomas, T.R. Dafforn, Encapsulated membrane proteins: a simplified system for molecular simulation, Biochim. Biophys. Acta Biomembr. 1858 (10) (2016) 2549–2557.
[3] Z. Hu, J.C.S. Ho, M. Nallani, Synthetic (polymer) biology (membrane): functionalization of polymer scaffolds for membrane proteins, Curr. Opin. Biotechnol. 46 (2017) 51–56.
[4] A.A. Gulamhussein, R. Uddin, B.J. Tighe, D.R. Poyner, A.J. Rothnie, A comparison of SMA (styrene maleic acid) and DIBMA (di-isobutylene maleic acid) for membrane protein purification, Biochim. Biophys. Acta Biomembr. 1862 (7) (2020), 183281.
[5] S. Gulati, M. Jamshad, T.J. Knowles, K.A. Morrison, R. Downing, N. Cant, R. Collins, J.B. Koenderink, R.C. Ford, M. Overduin, I.D. Kerr, T.R. Dafforn, A. J. Rothnie, Detergent-free purification of ABC (ATP-binding-cassette) transporters, Biochem. J. 461 (2) (2014) 269–278.
[6] A.C.K. Teo, S.C. Lee, N.L. Pollock, Z. Stroud, S. Hall, A. Thakker, A.R. Pitt, T. R. Dafforn, C.M. Spickett, D.I. Roper, Analysis of SMALP co-extracted phospholipids shows distinct membrane environments for three classes of bacterial membrane protein, Sci. Rep. 9 (1) (2019), 1813.
[7] J.P. Klare, E. Bordignon, M. Doebber, J. Fitter, J. Kriegsmann, I. Chizhov, H.-J. Steinhoff, M. Engelhard, Effects of Solubilization on the structure and function of the sensory rhodopsin II/transducer complex, J. Mol. Biol. 356 (5) (2006) 1207–1221.
[8] M. Zoonens, J. Comer, S. Masscheleyn, E. Pebay-Peyroula, C. Chipot, B. Miroux, F. Dehez, Dangerous liaisons between detergents and membrane proteins. The case of mitochondrial uncoupling protein 2, J. Am. Chem. Soc. 135 (40) (2013) 15174–15182.
[9] A.O. Oluwole, J. Klingler, B. Danielczak, J.O. Babalola, C. Vargas, G. Pabst, S. Keller, Formation of lipid-bilayer Nanodiscs by Diisobutylene/maleic acid (DIBMA) copolymer, Langmuir 33 (50) (2017) 14378–14388.
[10] R. Cuevas Arenas, J. Klingler, C. Vargas, S. Keller, Influence of lipid bilayer properties on nanodisc formation mediated by styrene/maleic acid copolymers, Nanoscale 8 (32) (2016) 15016–15026.
[11] C. Sun, R.B. Gennis, Single-particle cryo-EM studies of transmembrane proteins in SMA copolymer nanodiscs, Chem. Phys. Lipids 221 (2019) 114–119.
[12] C. Sun, S. Benlekbir, P. Venkatakrishnan, Y. Wang, S. Hong, J. Hosler, E. Tajkhorshid, J.L. Rubinstein, R.B. Gennis, Structure of the alternative complex III in a supercomplex with cytochrome oxidase, Nature 557 (7703) (2018) 123–126.
[13] J.M. Dörr, S. Scheidelaar, M.C. Koorengevel, J.J. Dominguez, M. Schäfer, C.A. van Walree, J.A. Killian, The styrene–maleic acid copolymer: a versatile tool in membrane research, Eur. Biophys. J. 45 (1) (2016) 3–21.
[14] N.L. Pollock, S.C. Lee, J.H. Patel, A.A. Gulamhussein, A.J. Rothnie, Structure and function of membrane proteins encapsulated in a polymer-bound lipid bilayer, Biochim. Biophys. Acta Biomembr. 1860 (4) (2018) 809–817.
[15] A. Colbasevici, N. Voskoboynikova, P.S. Orekhov, M.E. Bozdaganyan, M. G. Karlova, O.S. Sokolova, J.P. Klare, A.Y. Mulkidjanian, K.V. Shaitan, H.-J. Steinhoff, Lipid dynamics in nanoparticles formed by maleic acid-containing copolymers: EPR spectroscopy and molecular dynamics simulations, Biochim. Biophys. Acta Biomembr. 1862 (5) (2020), 183207.
[16] A.O. Oluwole, B. Danielczak, A. Meister, J.O. Babalola, C. Vargas, S. Keller, Solubilization of membrane proteins into functional lipid-bilayer Nanodiscs using a Diisobutylene/maleic acid copolymer, Angew. Chem. Int. Ed. 56 (7) (2017) 1919–1924.
[17] M. Overduin, M. Esmaili, Structures and interactions of transmembrane targets in native nanodiscs, SLAS DISCOVERY: Advancing the Science of Drug Discovery 24 (10) (2019) 943–952.
[18] E. van den Brink-van der Laan, J. Antoinette Killian, B. de Kruijff, Nonbilayer lipids affect peripheral and integral membrane proteins via changes in the lateral pressure profile, Biochim. Biophys. Acta Biomembr. 1666 (1) (2004) 275–288.
[19] M. Bogdanov, J. Xie, W. Dowhan, Lipid-protein interactions drive membrane protein topogenesis in accordance with the positive inside rule, J. Biol. Chem. 284 (15) (2009) 9637–9641.
[20] T. Heimburg, Physical Properties of Biological Membranes, Digital Encyclopedia of Applied Physics, 2009.
[21] A. Zachowski, Phospholipids in animal eukaryotic membranes: transverse asymmetry and movement, Biochem. J. 294 (Pt 1) (1993) 1–14.
[22] W. Mosslehy, N. Voskoboynikova, A. Colbasevici, A. Ricke, D. Klose, J.P. Klare, A. Y. Mulkidjanian, H.-J. Steinhoff, Conformational dynamics of sensory rhodopsin II in Nanolipoprotein and styrene–maleic acid lipid particles, Photochem. Photobiol. 95 (5) (2019) 1195–1204.
[23] K. Shimono, M. Iwamoto, M. Sumi, N. Kamo, Functional expression of pharaonis phoborhodopsin in Escherichia coli, FEBS Lett. 420 (1) (1997) 54–56.
[24] I.P. Hohenfeld, A.A. Wegener, M. Engelhard, Purification of histidine tagged bacteriorhodopsin, pharaonis halorhodopsin and pharaonis sensory rhodopsin II functionally expressed in Escherichia coli, FEBS Lett. 442 (2–3) (1999) 198–202.
[25] N. Mennes, J.P. Klare, I. Chizhov, R. Seidel, R. Schlesinger, M. Engelhard, Expression of the halobacterial transducer protein HtrII from Natronomonas pharaonis in Escherichia coli, FEBS Lett. 581 (7) (2007) 1487–1494.
[26] J. Schindelin, I. Arganda-Carreras, E. Frise, V. Kaynig, M. Longair, T. Pietzsch, S. Preibisch, C. Rueden, S. Saalfeld, B. Schmid, J.-Y. Tinevez, D.J. White, V. Hartenstein, K. Eliceiri, P. Tomancak, A. Cardona, Fiji: an open-source platform for biological-image analysis, Nat. Methods 9 (7) (2012) 676–682.
[27] D. Klose, N. Voskoboynikova, I. Orban-Glass, C. Rickert, M. Engelhard, J.P. Klare, H.-J. Steinhoff, Light-induced switching of HAMP domain conformation and dynamics revealed by time-resolved EPR spectroscopy, FEBS Lett. 588 (21) (2014) 3970–3976.
[28] J. Holterhues, E. Bordignon, D. Klose, C. Rickert, Johann P. Klare, S. Martell, L. Li, M. Engelhard, H.-J. Steinhoff, The signal transfer from the receptor NpSRII to the transducer NpHtrII is not hampered by the D75N mutation, Biophys. J. 100 (9) (2011) 2275–2282.
[29] R. Adão, P.F. Cruz, D.C. Vaz, F. Fonseca, J.N. Pedersen, F. Ferreira-da-Silva, R.M. M. Brito, C.H.I. Ramos, D. Otzen, S. Keller, M. Bastos, DIBMA nanodiscs keep α-synuclein folded, Biochim. Biophys. Acta Biomembr. 1862 (9) (2020), 183314.
[30] I. Chizhov, G. Schmies, R. Seidel, J.R. Sydor, B. Lüttenberg, M. Engelhard, The photophobic receptor from Natronobacterium pharaonis: temperature and pH dependencies of the photocycle of sensory rhodopsin II, Biophys. J. 75 (2) (1998) 999–1009.
[31] G. Schmies, B. Lüttenberg, I. Chizhov, M. Engelhard, A. Becker, E. Bamberg, Sensory rhodopsin II from the Haloalkaliphilic Natronobacterium pharaonis: light-activated proton transfer reactions, Biophys. J. 78 (2) (2000) 967–976.

[32] A.-A. Wegener, I. Chizhov, M. Engelhard, H.-J. Steinhoff, Time-resolved detection of transient movement of helix F in spin-labelled pharaonis sensory rhodopsin II11Edited by W. Baumeister, J. Mol. Biol. 301 (4) (2000) 881–891.
[33] F. Hagn, M.L. Nasr, G. Wagner, Assembly of phospholipid nanodiscs of controlled size for structural studies of membrane proteins by NMR, Nat. Protoc. 13 (1) (2018) 79–98.
[34] C.R. Harwood, D.A. Sykes, B. Hoare, F.M. Heydenreich, R. Uddin, D.R. Poyner, S. J. Briddon, D.B. Veprintsev, Functional solubilisation of the β_2−adrenoceptor (β_2AR) using Diisobutylene maleic acid (DIBMA), bioRxiv (2020) (2020.06.29.171512).
[35] M. Barniol-Xicota, S.H.L. Verhelst, Stable and functional rhomboid proteases in lipid Nanodiscs by using Diisobutylene/maleic acid copolymers, J. Am. Chem. Soc. 140 (44) (2018) 14557–14561.
[36] P. Stepien, A. Polit, A. Wisniewska-Becker, Comparative EPR studies on lipid bilayer properties in nanodiscs and liposomes, Biochim. Biophys. Acta Biomembr. 1848 (1, Part A) (2015) 60–66.
[37] M.C. Orwick, P.J. Judge, J. Procek, L. Lindholm, A. Graziadei, A. Engel, G. Gröbner, A. Watts, Detergent-free formation and physicochemical characterization of Nanosized lipid–polymer complexes: Lipodisq, Angew. Chem. Int. Ed. 51 (19) (2012) 4653–4657.
[38] A.P. Bali, I.D. Sahu, A.F. Craig, E.E. Clark, K.M. Burridge, M.T. Dolan, C. Dabney-Smith, D. Konkolewicz, G.A. Lorigan, Structural characterization of styrene-maleic acid copolymer-lipid nanoparticles (SMALPs) using EPR spectroscopy, Chem. Phys. Lipids 220 (2019) 6–13.
[39] I.G. Denisov, Y.V. Grinkova, A.A. Lazarides, S.G. Sligar, Directed self-assembly of Monodisperse phospholipid bilayer Nanodiscs with controlled size, J. Am. Chem. Soc. 126 (11) (2004) 3477–3487.
[40] K. Cosentino, U. Ros, A.J. García-Sáez, Assembling the puzzle: Oligomerization of α-pore forming proteins in membranes, Biochim. Biophys. Acta Biomembr. 1858 (3) (2016) 457–466.
[41] A.J. Bell, L.K. Frankel, T.M. Bricker, High yield non-detergent isolation of photosystem I-light-harvesting chlorophyll II membranes from spinach thylakoids: IMPLICATIONS FOR THE ORGANIZATION OF THE PS I ANTENNAE IN HIGHER PLANTS, J. Biol. Chem. 290 (30) (2015) 18429–18437.
[42] E. Häusler, K. Fredriksson, I. Goba, C. Peters, K. Raltchev, L. Sperl, A. Steiner, S. Weinkauf, F. Hagn, Quantifying the insertion of membrane proteins into lipid bilayer nanodiscs using a fusion protein strategy, Biochim. Biophys. Acta Biomembr. 1862 (4) (2020), 183190.